Applied Catalysis B: Environmental 182 (2016) 26–32

Contents lists available at ScienceDirect

Applied Catalysis B: Environmental

journal homepage: www.elsevier.com/locate/apcatb

Visible light photocatalytic activity enhancement of Ag_3PO_4 dispersed on exfoliated bentonite for degradation of rhodamine B

Jianfeng Ma[a,b], Qing Liu[a], Lifang Zhu[c], Jing Zou[a], Kai Wang[a], Meirong Yang[a], Sridhar Komarneni[b,*]

[a] School of Environmental and Safety Engineering, Changzhou University, Jiangsu 213164, China
[b] Materials Research Laboratory, Materials Research Institute, The Pennsylvania State University, University Park, PA 16802, USA
[c] Zhejiang University of Water Resources and Electric Power, Zhejiang 310018, China

ARTICLE INFO

Article history:
Received 27 March 2015
Received in revised form 30 August 2015
Accepted 4 September 2015
Available online 8 September 2015

Keywords:
Silver phosphate
Exfoliated bentonite
Visible light
Photocatalysis
Rhodamine B dye

ABSTRACT

To improve catalytic efficiency and reduce the amount of silver consumption, nanophase of silver phosphate was dispersed on an exfoliated bentonite (EB) to prepare the EB–Ag_3PO_4 photocatalyst. The as-synthesized samples were characterized by X-ray diffraction (XRD), Transmission electron microscopy (TEM), Fourier transform infrared spectroscopy (FTIR), Ultraviolet–vis (UV–vis) diffuse reflectance spectroscopy (DRS) and the Brunauer, Emmett, and Teller (BET) method. The composites were obtained with very fine nanoparticles of Ag_3PO_4 spread on the thin layers of exfoliated bentonite in order to improve the photocatalytic activity by exposing higher surface area of Ag_3PO_4. An optimized EB–Ag_3PO_4 composite showed much higher degradation of rhodamine B than that of the pure Ag_3PO_4 under visible light irradiation on a per mole basis of Ag_3PO_4. In addition, degradation efficiency of Ag_3PO_4 was apparently improved by compositing with exfoliated bentonite based on the kinetics of degradation data. The RhB degradation by EB–Ag_3PO_4-3 composite reached about 95% within 21 min under visible light irradiation, which is much higher than that of Ag_3PO_4 (82%). The results of improved photoactivity were mainly attributed to the electrostatic interaction between Ag_3PO_4 and negatively charged exfoliated bentonite, efficient migration of the photogenerated electrons and holes occurred in nanocomposite. This study reports a highly efficient and cost-effective photocatalyst for dye pollutant degradation and a potential photoelectric material.

1. Introduction

Semiconductor-assisted photodegradation of organic pollutants has been receiving a lot of attention because it is an economic and eco-friendly solution for the remediation of environmental pollution with dyes. Recently, silver orthophosphate (Ag_3PO_4) has been discovered as a novel and highly active visible-light photocatalyst due to the efficient separation of photoexcited electrons and holes [1]. Intriguingly, Ag_3PO_4 has extremely high photooxidative capabilities for the evolution of O_2 from water splitting and for the decolorization of organic dyes under visible light irradiation [2]. Ag_3PO_4 has a suitable band gap of 2.45 eV and can achieve a quantum yield of up to 90% at wavelengths longer than 520 nm, which is significantly higher than that of other semiconductors reported in the literature [3]. Therefore, Ag_3PO_4 has been touted as one of the most promising photocatalysts in harvesting solar energy for environmental purification and clean energy production. Moreover, the photocatalytic activity of Ag_3PO_4 can be further improved by controlling shape [4], morphology [5] and crystal face [6] of Ag_3PO_4 crystals, and by compositing with other materials, which include semiconductors such as $BiPO_4$ [7], Fe_3O_4 [8], AgBr [9], ZnO [10], SnO_2 [11],TiO_2 [12], etc., and carbon materials including graphene [13], oxidized graphene [14] and carbon quantum dots [15]. Therefore, it is very important to search for cost-effective and efficient materials to further improve Ag_3PO_4 catalyst.

Due to low cost, abundant availability, easy accessibility and environmentally friendly nature, bentonite clay represents an appealing substrate for depositing all kinds of photocatalysts. Bentonite is an industrial name for montmorillonite clay. Montmorillonite is a phyllosilicate mineral consisting of 2:1 stacked layers with two tetrahedral sheets sandwiching an octahedral sheet and possessing a swelling behavior [16,17]. The isomorphous substitution of Al^{3+} for Si^{4+} in the tetrahedral sheet and/or Mg^{2+} or Zn^{2+} for Al^{3+} in the octahedral sheet results in a net negative charge

* Corresponding author. Fax: +1 814 865 2326.
E-mail address: sxk7@psu.edu (S. Komarneni).

http://dx.doi.org/10.1016/j.apcatb.2015.09.004
0926-3373/

on the clay surface [18]. Compared with other clays, bentonite has excellent adsorption capacities and possesses sorption/exchange sites available within its interlayer space as well as on the outside surfaces and edges [19]. For the above reasons, bentonite is the most effective adsorbent used in removal of dyes [20]. Besides, many studies have shown that bentonite is a good substrate for synthesis of composite photocatalysts with higher photocatalytic activity, for examples, CdS/bentonite [21], ZnS/bentonite [22], TiO_2/bentonite [12], g-C_3N_4/bentonite [23], $BiVO_4$/bentonite [24] and MoS_2/bentonite [25] were previously tested. All of these composite photocatalysts showed stronger ability for degradation of organic pollutants because of uniform dispersion of photocatalyst on the clay substrate generating distinct reaction sites. Furthermore, all synthetic composites of bentonite showed greater specific surface area and improved adsorption property, which resulted in higher photocatalytic performance compared to pure catalysts as single phases. By dispersing on a substrate, the amount of photocatalyst needed for degradation of organic pollutants is also reduced.

In our previous study, the silver salt was intercalated into bentonite interlayers for the synthesis of Ag_3PO_4–Ben composites and they exhibited high catalytic efficiency for Orange II degradation under visible light irradiation. However, catalyst loaded in the interlayer is not conducive to the absorption of the photons. If the bentonite is exfoliated and the photocatalytic nanoparticles were to be supported on exfoliated bentonite nano-layer external surfaces, they will lead to better photocatalytic effect [26]. Therefore, in this study, we assembled Ag_3PO_4 nanocrystals on exfoliated bentonite nanolayers in order to produce exfoliated bentonite-Ag_3PO_4 (EB–Ag_3PO_4) nanocomposites for improving the photocatalytic activity of this visible light-responsive photocatalyst. After exfoliating of bentonite, the huge internal surface area of bentonite is exposed to the outside. Thus, the external surface area of the bentonite can be greatly increased by exfoliation, which in turn enhances the adsorption performance and promotes the catalyst's role. The work reported here, demonstrates a facile strategy to synthesize EB–Ag_3PO_4 composites and its application for photocatalytic degradation of organic dyes in water under visible light irradiation. The composition, morphology, and optical properties of the as-synthesized EB–Ag_3PO_4 composites were characterized. The photocatalytic performance of EB–Ag_3PO_4 composites was evaluated by the photo-degradation of rhodamine B (RhB) in water under visible light. The effects of exfoliated bentonite amounts in composites on the visible-light-driven photocatalytic efficiency were investigated. Moreover, a possible mechanism for degradation of RhB over EB–Ag_3PO_4 composite was proposed based on the present experimental results.

2. Experimental

2.1. Preparation of photocatalysts

All chemicals were of analytical grade and used without further purification. Natural bentonite, composed primarily of Ca^{2+}-montmorillonite, is obtained from Tianyu Co., Ltd. (Inner Mongolia, China). Its structural formula is $Ca_{0.392}Na_{0.016}K_{0.020}(Si_{7.92}Al_{0.08})(Al_{2.518}Fe_{0.450}Mg_{1.104}Ti_{0.036}Mn_{0.004})O_{10}(OH)_2{\cdot}nH_2O$, and the charge density is $-0.82\,e$ per unit cell. The total cationic exchange capacity (CEC) is 108 meq/100 g [27]. The natural bentonite was ground and sieved by 200-mesh then washed with distilled water for 3–4 times. Silica and Iron oxides were removed by differential sedimentation technique. The mixture was stirred for 1 h and then kept undisturbed overnight. After filtration to separate the solid and solution, the solid was dried at room temperature. Exfoliation of bentonite was carried out by liquid phase stripping as follows: 10 g bentonite clay was mixed in 200 mL water containing 0.4 g of NaF and the mixture was stirred for 90 min at 80 °C. Then 0.05 g $(NaPO_3)_6$ was added to the above mixture and the whole present mixture was transferred to a high-speed dispersion machine. After the high-speed dispersion for 30 min, the mixture was ultrasonicated for 30 min. Then the mixture was kept undisturbed for 1 day and followed by its centrifugation at 7000 rpm for 30 min in order to separate a colloidal fraction. After centrifugation, the supernatant contained the colloidal fraction, which was collected and designated as 'exfoliated bentonite'. The exfoliated bentonite was used in all the subsequent experiments.

A facile room temperature approach for the synthesis of EB–Ag_3PO_4 nanocomposites is depicted in Fig. 1. The overall synthetic procedure consists of a two-stage nucleation-growth process. Firstly, 100 mL aqueous suspension of exfoliated bentonite

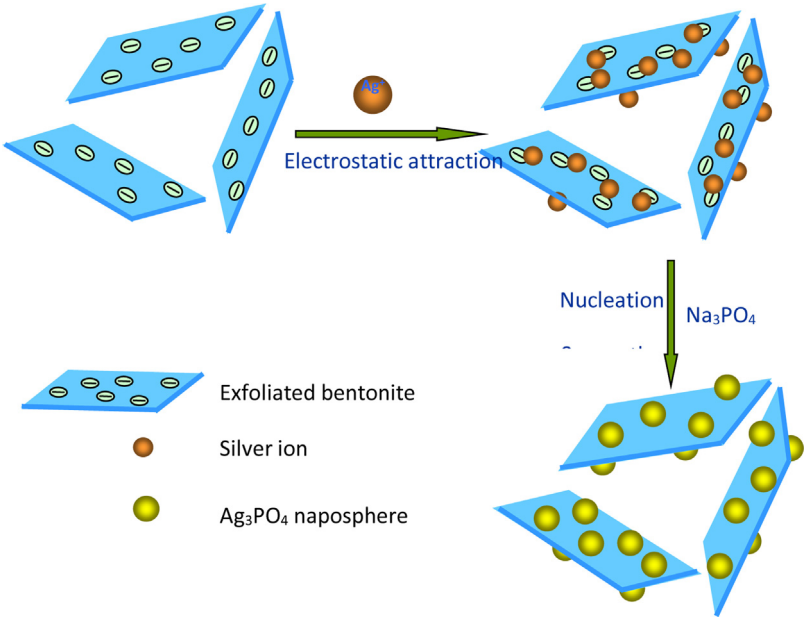

Fig. 1. Schematic illustration of the formation process of EB–Ag_3PO_4 nanocomposites.

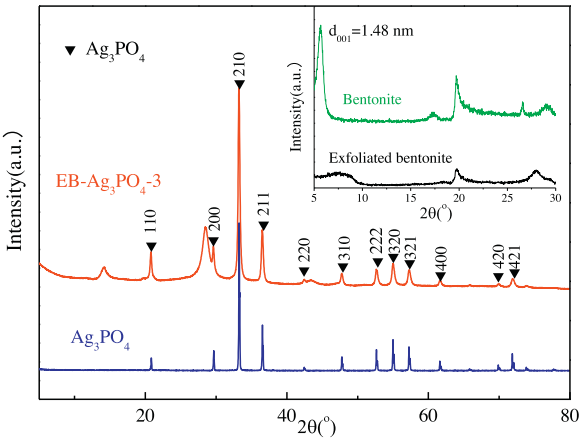

Fig. 2. X-ray diffraction patterns of Ag_3PO_4 and EB–Ag_3PO_4-3. In the EB–Ag_3PO_4-3 pattern two additional minor phases were detected. The peak at about $2\theta = 13^\circ$ is characteristic to $CaNaPO_4$ and the peak at about $2\theta = 28.3^\circ$ is characteristic to $CaAgPO_4$. Low-angle X-ray diffraction patterns of natural bentonite and exfoliated bentonite are shown in the inset.

(10 g/L) was mixed with $AgNO_3$ solution and stirred for 30 min at room temperature. Because of the electrostatic interaction between Ag^+ and exfoliated bentonite in aqueous solution, the positively charged Ag^+ ions can easily exchange onto the surface of negatively charged exfoliated bentonite nanosheets during this process, as schematically shown in Fig. 1. Then, Na_3PO_4 aqueous solution was added dropwise to the mixture, the PO_4^{3-} anions reacted with silver cations on the exfoliated bentonite leading to the formation of Ag_3PO_4 nuclei at the interaction sites between Ag^+ and exfoliated bentonite while the Na^+ ions occupied the negative sites on clay. The exfoliated bentonite keeps the concentration of Ag^+ in the solution low and thus slows down the nucleation rate of Ag_3PO_4 by forming the intermediate Ag^+-exfoliated bentonite complexes. As the reaction proceeded, these nuclei slowly grew and were transformed into larger Ag_3PO_4 nanoparticles after the Ostwald ripening process. During the course of reaction, the color of the mixture gradually changed from bright yellow to brownish. This alteration in color indicated the formation of Ag_3PO_4 nanoparticles in the suspension. After 2 h of reaction, the color of the mixture did not change, suggesting that Ag^+ ions were completely consumed and Ag_3PO_4 nanospheres were successfully loaded onto the exfoliated bentonite. Finally, the products were collected by centrifugation and washed several times with distilled water and ethyl alcohol, and then dried in a vacuum oven at 55 °C. The amounts of initially added $AgNO_3$ were 2, 3 and 4 mmol, and the obtained samples are labeled as EB–Ag_3PO_4-2, EB–Ag_3PO_4-3 and EB–Ag_3PO_4-4, respectively. For comparison purpose, pure Ag_3PO_4 nanoparticles were synthesized without the addition of aqueous suspension of exfoliated bentonite. The Ben–Ag_3PO_4 was synthesized using a similar process by adding 3 mmol $AgNO_3$ to the natural bentonite. Exfoliated bentonite and Ag_3PO_4 mechanical mixture was prepared by mixing aqueous suspension of exfoliated bentonite (100 mL, 10 g/L) with pure Ag_3PO_4 (1 mmol), stirring for 30 min at room temperature, centrifuging to separate the solid from solution and collecting the solid. This solid was dried in a vacuum oven at 55 °C and it was denoted as EB–Ag_3PO_4 mixture.

2.2. Characterization

X-ray diffraction (XRD) patterns of the prepared samples were determined by using an X-ray diffractometer (Max-2550PC, Rigaku D) with Cu Kα radiation (40 kV, 300 mA) of 0.154 nm wavelength to confirm the crystalline nature of the materials. Ultraviolet–vis (UV–vis) diffuse reflectance spectra were recorded using a UV–vis spectrometer (UV-2450, Shimadzu) and converted to absorption spectra by the standard Kubelka–Munk method. Fourier transform infrared (FTIR) spectra were obtained using the KBr pressed disk technique on a Thermo Nicolet Nexus 670 FTIR spectrophotometer. The FTIR spectra in the range of 4000–400 cm^{-1} were recorded with a resolution of 4 cm^{-1}, and 64 interferograms were collected. Transmission electron microscopy (TEM) was performed on the exfoliated bentonite and EB–Ag_3PO_4-3 by JEOL JEM-2100 LaB6 transmission electron microscope (Japan). Specific surface areas of the prepared photocatalysts were measured using the Brunauer, Emmett, and Teller (BET) method (Autosorb-iQ2-MP, Quantachrome Instruments).

2.3. Photocatalytic activity testing

The photocatalytic activity of EB–Ag_3PO_4 composites was evaluated by photodegradation of RhB dye in aqueous solution. The visible light source used in the measurements was 5 × 24W LED lamps. A 0.2 g of powdered photocatalyst was added into 200 mL RhB aqueous solution (20 mg/L). Visible-light irradiation was conducted after the suspension was magnetically stirred in the dark for 60 min to reach adsorption–desorption equilibrium. During irradiation, 3 mL aliquots were sampled at the given time intervals and centrifuged to remove the photocatalyst. The resulting clear liquor was analyzed on a UV–vis spectrophotometer (UV-2450, Shimadzu, Japan) to record the concentration changes of RhB. The percentage

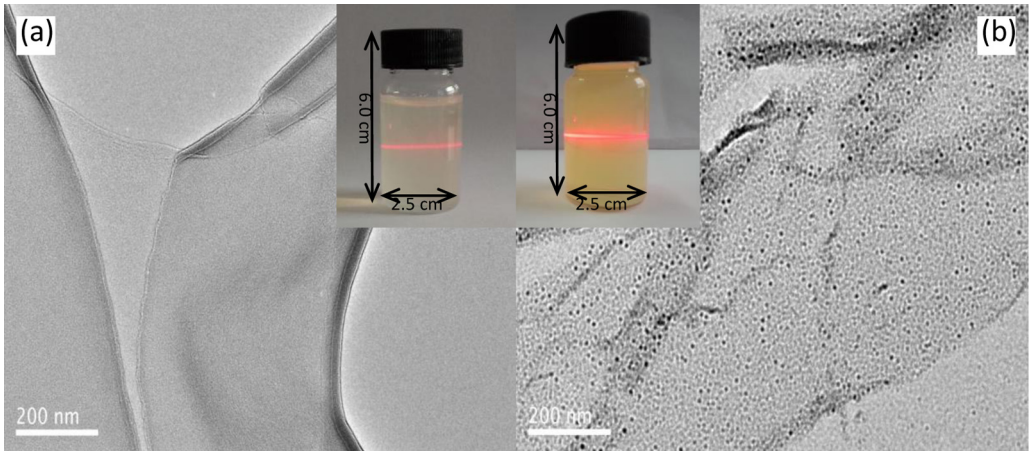

Fig. 3. TEM images of (a) exfoliated bentonite and (b) EB–Ag_3PO_4-3 composite. Tyndall effect of colloidal solution of exfoliated bentonite and EB–Ag_3PO_4-3 are shown in the inset.

of degradation is reported as C/C_0. C is the absorption of RhB at each irradiated time interval of the main peak of the absorption spectrum at 554 nm, and C_0 is the absorption of the initial concentration.

The processes for evaluation of the stability and recyclability of the composites were conducted as follows: at the end of each cycle, the suspension was centrifuged and the supernatant was analyzed and discarded. The dose of photocatalyst was 1 g/L. When H_2O_2 was added, the H_2O_2 (30%) amount was 100 μL per liter of RhB solution.

3. Results and discussion

3.1. XRD analysis

The samples of natural bentonite, exfoliated bentonite, pure Ag_3PO_4 and EB–Ag_3PO_4-3 composite were characterized by XRD and their patterns are presented in Fig. 2. According to the XRD pattern of natural bentonite, the predominant peak at $2\theta = 5.64^\circ$ gives the c-axis dimension of 1.48 nm, which is characteristic to montmorillonite. For exfoliated bentonite, the characteristic peak of bentonite at 2θ is broad and weak as expected, which suggested that the layers of bentonite clay were delaminated by exfoliation. For the pattern of pure Ag_3PO_4, all of the diffraction peaks can be readily indexed to the cubic phase of Ag_3PO_4 (JCPDS No. 06-0505). In addition, the EB–Ag_3PO_4-3 exhibited a coexistence of both exfoliated bentonite and Ag_3PO_4 phases, confirming the formation of EB–Ag_3PO_4 composites. The results also illustrate that the incorporation of Ag_3PO_4 on exfoliated bentonite had no effect on the crystal structure of Ag_3PO_4. In the EB–Ag_3PO_4-3 pattern (Fig. 2) two additional minor phases were detected. The peak at about $2\theta = 13^0$ is characteristic to $CaNaPO_4$ in a very small amount which is produced during the synthesis of EB–Ag_3PO_4 when the $(NaPO_3)_6$ was added. The peak at about $2\theta = 28.3^0$ is characteristic to $CaAgPO_4$ (Fig. 2). The calcium silver phosphate was probably produced by direct reaction with Ca or from $CaNaPO_4$. In this system, bentonite was the calcium source because Ca existed as the exchangeable ion.

3.2. TEM analysis

The morphology of exfoliated bentonite and EB–Ag_3PO_4-3 was investigated by TEM. The layered structure of natural bentonite had been stripped into ultrathin layers (Fig. 3a), which might provide enough surface area to not only adsorb pollutants but also in close contact with Ag_3PO_4 nanospheres in the EB–Ag_3PO_4 composites. Fig. 3b shows light-gray films, which are the exfoliated bentonite layers, and the small black spots on the layers are the Ag_3PO_4 nanospheres. The exfoliated bentonite sheets were evenly and densely decorated with uniform Ag_3PO_4 nanospheres of approximately 6–8 nm in size. These Ag_3PO_4 nanospheres were firmly bound to exfoliated bentonite sheets even though extensive sonication and washing was done for dispersing the sample before TEM characterization. This indicates the strong bonding between Ag_3PO_4 nanospheres and exfoliated bentonite layers. Thus, TEM observations also verified the successful synthesis of exfoliated bentonite and Ag_3PO_4 nanospheres as a nanocomposite. In addition, two insets in Fig. 3 show reflected colloidal solutions of exfoliated bentonite and EB–Ag_3PO_4-3 with Tyndall effect: when the red laser light passes through the colloidal solution, it is scattered and becomes visible. This is further evidence that the bentonite used in this study consisted of exfoliated layers.

3.3. FTIR analysis

The FTIR spectra of exfoliated bentonite, pure Ag_3PO_4 and EB–Ag_3PO_4-3, which were recorded from 400 cm^{-1} to 4000 cm^{-1} are shown in Fig. 4 for comparison with each other. The broad

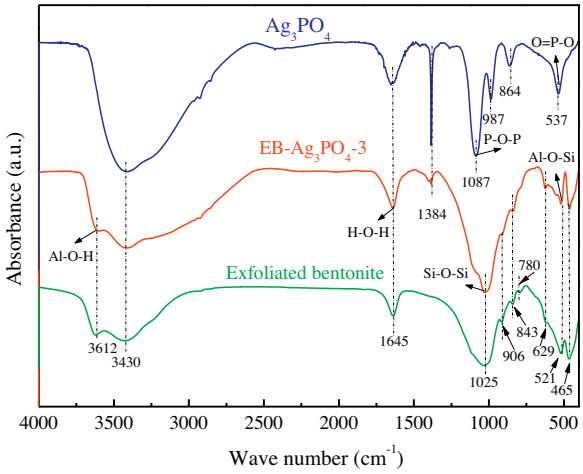

Fig. 4. FTIR spectra of exfoliated bentonite, Ag_3PO_4 and EB–Ag_3PO_4-3 composite.

absorption peaks around 3430 cm^{-1} are assigned to the stretching vibration of O—H groups and the bands at about 1645 cm^{-1} are attributed to H—O—H bending vibrations of adsorbed H_2O. For the spectrum of exfoliated bentonite, the peak at 3612 cm^{-1} corresponds to Al—O—H stretching vibration. Strong band at 1025 cm^{-1} is related to the stretching vibrations of Si—O—Si bonds, which are characteristic of phyllosilicate minerals. The bands at 465 and 521 cm^{-1} correspond to Si—O—Si and Al—O—Si bending vibrations. The band at 629 cm^{-1} is assigned to the out-of-plane vibrations of coupled Al—O and Si—O. The band at 780 cm^{-1} confirmed quartz admixture in the sample. The band at 843 cm^{-1} is assigned to the bending vibration of AlMgOH. The spectral band at 906 cm^{-1} reflects the stretching vibration of Al—O—(OH—Al [28]. For pure Ag_3PO_4, the band at about 537 cm^{-1} is assigned to O=P—O bending vibration, while the band at 864 cm^{-1} is due to the symmetric stretching vibration of P—O—P rings. One strong band at 1087 cm^{-1} comes from the asymmetric stretching of P—O—P groups [29]. The sharp peak at about 1384 cm^{-1} is from nitrate impurities as $AgNO_3$ precursor was used for the preparation of Ag_3PO_4 and the lower intensity of this peak in the EB–Ag_3PO_4 is because only 2–4 mmol of silver nitrate was used for Ag_3PO_4 loading in each gram of exfoliated bentonite. In contrast, the spectrum of the EB–Ag_3PO_4-3 composite, showed a band at approximately 3430 cm^{-1} that is wider than those of exfoliated bentonite and pure Ag_3PO_4, apparently due to the charge interactions between exfoliated bentonite and pure Ag_3PO_4 in the former. All the characteristic peaks of exfoliated bentonite and pure Ag_3PO_4 were observed in the EB–Ag_3PO_4-3 hybrid composite photocatalysts, suggesting that Ag_3PO_4 nanospheres have been successfully attached to the exfoliated bentonite.

3.4. BET analysis

In order to investigate any changes to the surface property of the EB–Ag_3PO_4 composite after Ag_3PO_4 was dispersed on exfoliated bentonite, the BET surface areas of exfoliated bentonite, pure Ag_3PO_4 and EB–Ag_3PO_4-3 composite were determined. The BET surface areas of exfoliated bentonite and pure Ag_3PO_4 were 79.6 $m^2\,g^{-1}$ and 23.5 $m^2\,g^{-1}$, respectively while the specific surface area of the EB–Ag_3PO_4-3 composite was 76.2 $m^2\,g^{-1}$, which suggests that deposition of 2/3–4/3 mmol of nano Ag_3PO_4 on each gram of exfoliated bentonite did not decrease the surface area of the composite significantly. The high surface area retained in the composite is beneficial for the enhancement of photocatalyst's activity. Previous studies also reported higher BET surface areas of the composites in g-C_3N_4/bentonite [23] and TiO_2/bentonite [30] systems after g-C_3N_4 and TiO_2 were loaded on to the bentonite

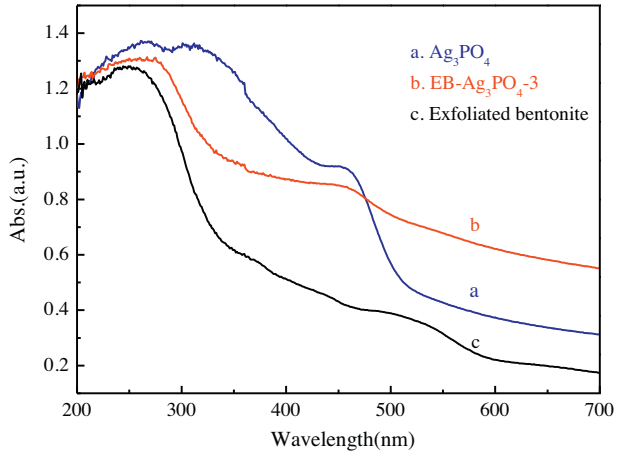

Fig. 5. UV–vis absorption spectra of exfoliated bentonite, Ag_3PO_4 and EB–Ag_3PO_4-3 composite.

clay. This means that Ag_3PO_4 dispersed on exfoliated bentonite i.e., EB–Ag_3PO_4 composite with high BET surface area is expected to be a good photocatalyst.

3.5. UV–vis DRS

The optical absorption property of photocatalyst is a key factor that determined its photocatalytic performance [31]. The UV–vis DRS of pure Ag_3PO_4, exfoliated bentonite, and EB–Ag_3PO_4-3 were collected and the results are shown in Fig. 5. Pure Ag_3PO_4 showed strong absorption with absorption edge at about 530 nm, which is in agreement with the results reported previously. Exfoliated bentonite shows little absorption in the range of visible light (Fig. 5). However, with the loading of Ag_3PO_4 on EB, the absorption edge of EB–Ag_3PO_4-3 was not shifted, but the absorbance in the range of 500–700 nm was enhanced in comparison with that of pure Ag_3PO_4. This implied that EB–Ag_3PO_4-3 might use solar spectrum more efficiently leading to higher photocatalytic activity. Similar phenomena have been observed in the case of GO–Ag_3PO_4 composite [32] and Ag_3PO_4–SBA-15 composite [33].

3.6. Photocatalytic performance testing

The photocatalytic activities of EB–Ag_3PO_4 composites were mainly evaluated by photocatalytic degradation of RhB aqueous solution under visible light irradiation. Temporal concentration changes of RhB were monitored by examining the variations in maximal absorption in UV–vis spectra at 554 nm. In order to investigate the influence of Ag_3PO_4 content on the photocatalytic activity, pure Ag_3PO_4 and EB–Ag_3PO_4 composites with different contents of Ag_3PO_4 were used to decompose RhB dye. Fig. 6a shows the photocatalytic activity of the pure Ag_3PO_4, exfoliated bentonite, Ben–Ag_3PO_4, EB–Ag_3PO_4-2, EB–Ag_3PO_4-3, EB–Ag_3PO_4-4 and EB–Ag_3PO_4 physical mixture under visible-light irradiation. Prior to irradiation, the RhB solution containing the catalyst was kept in the dark for 60 min to obtain the equilibrium adsorption state. In the dark, about 50% of RhB has been adsorbed by EB–Ag_3PO_4 composite photocatalysts, while the amount of RhB absorbed by pure Ag_3PO_4 is only 15%, showing the high adsorption capacity of exfoliated bentonite (Fig. 6a). The charge-based interaction between negatively charged exfoliated bentonite nanolayers and the cationic RhB dye is believed to be responsible for the high adsorption capacity. The concentration of RhB decreased gradually as the exposure time increased for all samples except for exfoliated bentonite, as expected. These results

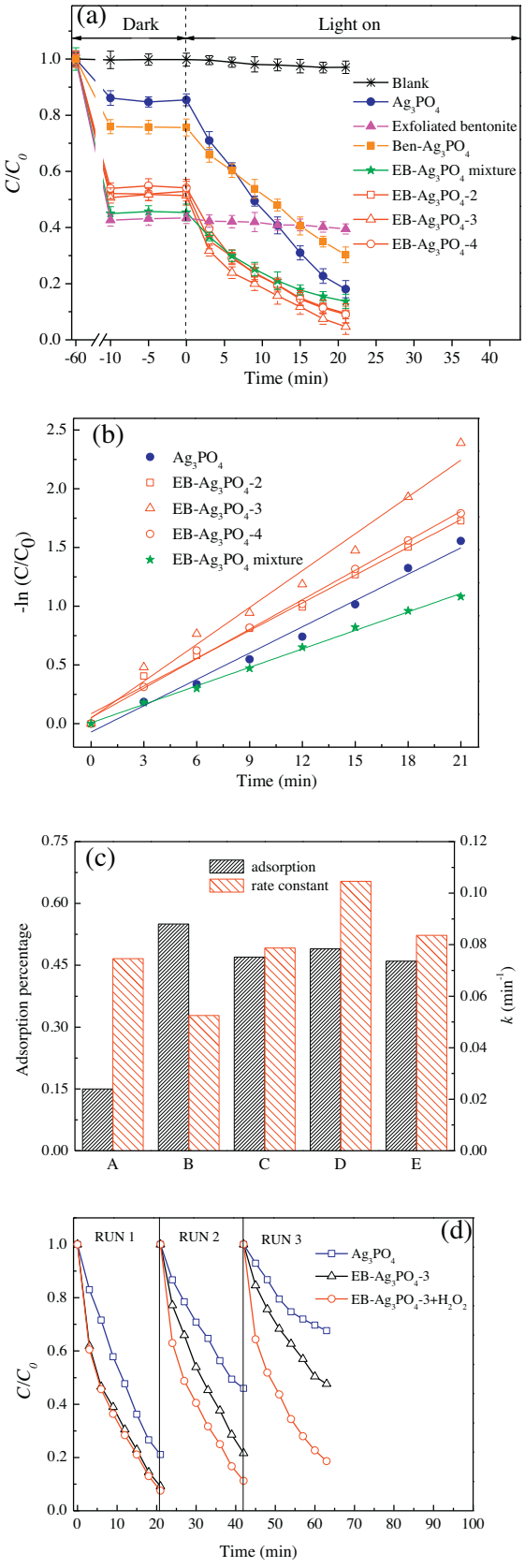

Fig. 6. (a) Photocatalytic degradation of RhB by Ag_3PO_4, exfoliated bentonite, Ben–Ag_3PO_4, EB–Ag_3PO_4 mixture and EB–Ag_3PO_4 composites, (b) kinetic fit for the degradation of RhB with Ag_3PO_4, EB–Ag_3PO_4 mixture and EB–Ag_3PO_4 composites, (c) adsorption activity and rate constants of (A) Ag_3PO_4, (B) EB–Ag_3PO_4 physical mixture, (C) EB–Ag_3PO_4-2, (D) EB–Ag_3PO_4-3 and (E) EB–Ag_3PO_4-4 composites, (d) cycling runs for the degradation of RhB with Ag_3PO_4, EB–Ag_3PO_4-3 and EB–Ag_3PO_4-3 + H_2O_2.

illustrate that the as-prepared pure Ag_3PO_4, Ben–Ag_3PO_4 and all EB–Ag_3PO_4 composites exhibited visible light responsive catalytic activities. Furthermore, the pure Ag_3PO_4 and Ben–Ag_3PO_4 showed poor photocatalytic activities compared with those of EB–Ag_3PO_4 composites on a per mole basis of Ag_3PO_4. During the 21-min reaction under visible light irradiation, the degradation ratio varied with the amount of added Ag_3PO_4 in the synthesis process as follows: EB–Ag_3PO_4-3 (95%) > EB–Ag_3PO_4-4 (91%) > EB–Ag_3PO_4-2 (90%) > EB–Ag_3PO_4 physical mixture (86%) > Ag_3PO_4 (82%). The enhanced photocatalytic activity of EB–Ag_3PO_4 composites can be ascribed to the high adsorption activity of the composite photocatalyst for RhB and the high migration efficiency of photo-induced electrons. However, there is an optimal value of Ag_3PO_4 amount, which was determined to be 3 mmol g^{-1} in our experiments.

The photocatalytic degradation of RhB over Ag_3PO_4 and EB–Ag_3PO_4 composites followed the pseudo-first-order kinetics (shown in Fig. 6b) by the formula below:

$$\ln\frac{C_t}{C_0} = -kt$$

In the above equation, k is kinetic constant. The average rate constants (k) for EB–Ag_3PO_4 composites with 2, 3 and 4 mmol g^{-1} Ag_3PO_4 content were estimated to be 0.08 min^{-1}, 0.10 min^{-1} and 0.08 min^{-1}, respectively, which are larger than those for pure Ag_3PO_4 (k = 0.07 min^{-1}) and EB–Ag_3PO_4 physical mixture (k = 0.05 min^{-1}) (Fig. 6b). These results revealed that the combination between exfoliated bentonite and Ag_3PO_4 could highly enhance the photocatalytic activity under visible light irradiation.

Adsorption makes a big difference in most photocatalytic reactions. Fig. 6c shows the comparison of the adsorption capacity and rate constants of all catalysts tested here during the degradation process. Compared with EB–Ag_3PO_4 physical mixture, the adsorption capacities of EB–Ag_3PO_4 composites were not higher although the rate constants are much higher. Note, EB–Ag_3PO_4-3 composite showed the optimal rate constant (0.1046 min^{-1}), which is around 2.0 times that of the EB–Ag_3PO_4 mixture (0.0525 min^{-1}). From these data, the higher degradation activity of EB–Ag_3PO_4 composites is not mainly ascribed to the adsorption capability alone. The enhanced photocatalytic activity can also be attributed to the significant differences in the interface of the samples, as the hybrid composites showed a closely contacted interface whereas only a diffuse interface can be formed in a simple mechanical mixture. It is well-known that Ag_3PO_4 is not so stable under the irradiation as it will be reduced to the Ag^0 without a sacrificial reagent [26]. The cycling degradation experiments of pure Ag_3PO_4 and EB–Ag_3PO_4-3 under visible light irradiation are shown in Fig. 6d. The effect of sacrificial reagent (H_2O_2) on rejuvenation was also evaluated. The photocatalytic stability of Ag_3PO_4 deteriorated greatly and the Ag_3PO_4 almost lost its activity after three successive cycles of RhB degradation. However, the EB–Ag_3PO_4-3 showed much higher removal efficiency and stability than the pure Ag_3PO_4 (Fig 6d). This result suggests that the presence of exfoliated bentonite is beneficial to inhibit silver reduction. Ag_3PO_4 can be rejuvenated by H_2O_2, compared with the system without any H_2O_2, the photocatalytic activity of the EB–Ag_3PO_4-3 + H_2O_2 was still as high as that of the fresh Ag_3PO_4 as the former could degrade 81% of RhB at the last run of the recycle.

3.7. Possible mechanism

Several reasons may account for the enhanced photocatalytic activity of the EB–Ag_3PO_4 photocatalysts. Firstly, the EB–Ag_3PO_4 photocatalysts exhibited more enhanced visible light photocatalytic efficiency than that of pure Ag_3PO_4, which indicates the composites can be excited by more visible light photons. Secondly, the smaller size (6–8 nm), uniformity and sphericity of

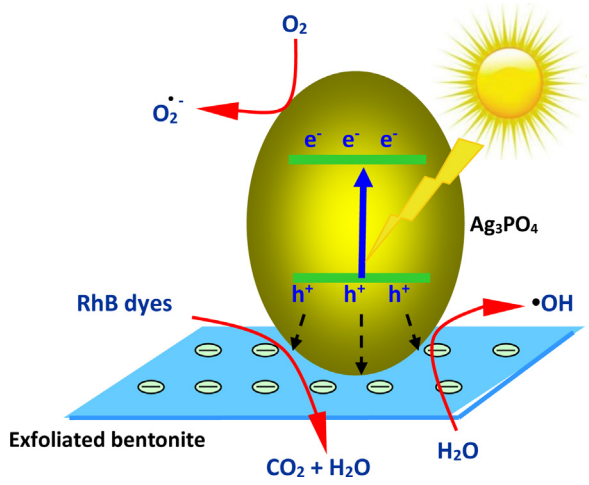

Fig. 7. Proposed mechanism for the photodegradation of RhB on EB–Ag_3PO_4 composites.

Ag_3PO_4 particles which provide more surface-to-volume ratio led to enhaced photocatalytic activity [34]. Thirdly, the larger BET surface of EB–Ag_3PO_4 photocatalysts provided more surface active sites for adsorption and photocatalytic reaction [35]. Fourthly, the improved adsorption of the RhB molecules by EB–Ag_3PO_4 photocatalysts compared with that of pure Ag_3PO_4 could accelerate the photodegradation reaction. Furthermore, the electrostatic interaction of the negatively charged exfoliated bentonite can promote the separation of electrons and holes and thus suppresses the charge recombination. A possible mechanism for the photodegradation of RhB over EB–Ag_3PO_4 photocatalyst is proposed in Fig. 7. It is a fact that bentonite is known to be a very good electrical insulator [36] and hence exfoliated bentonite can not be excited but only Ag_3PO_4 can be activated. Under visible light illumination, the valence band (VB) electrons (e^+) of Ag_3PO_4 can be easily excited to the conduction band (CB) by visible light photons ($h\nu$), inducing the formation of holes (h^+) in the VB [15]. The electrons–holes of Ag_3PO_4 have no opportunity to transfer to exfoliated bentonite and should still be present on Ag_3PO_4 surface. The excited electrons and holes of Ag_3PO_4 should be driven to migrate efficiently because of electrostatic repulsion between the negatively charged electron and the negatively charged exfoliated bentonite and electrostatic attraction between the positively charged hole and the negatively charged exfoliated bentonite. Therefore, the probability of electron–hole recombination can be decreased and hence more charge carriers are available to increase the photocatalytic activity. Likewise, previous studies with other insulator–semiconductor systems such as g-C_3N_4/bentonite composites [23] and hexagonal-BN/TiO_2 composites [37] led to improved photocatalytic activity because of electrostatic interactions. Holes react with water producing highly reactive hydroxyl radicals (•OH) and electrons can be trapped by the available surface O_2 to initiate the yield of reactive species such as anions ($O_2^{\bullet-}$), which react with H_2O yielding •OH active radical species as has been proposed previously [38]. Both $O_2^{\bullet-}$ and •OH radicals can effectively decompose RhB into CO_2, H_2O and other intermediates under visible light irradiation [39]. Furthermore, reactive holes are able to oxidize organic dye directly because of their strong oxidation ability [40].

4. Conclusions

In summary, an excellent hybrid photocatalyst of EB–Ag_3PO_4 was synthesized via a convenient in situ ion exchange route. XRD, TEM and FTIR revealed that Ag_3PO_4 nanospheres were successfully attached on to the surface of exfoliated bentonite. The uniform

Ag_3PO_4 nanospheres were evenly and densely spread on the exfoliated bentonite sheets with the diameter of about 6–8 nm, which resulted in improved photocatalytic activity. The RhB degradation by EB–Ag_3PO_4-3 composite reached about 95% within 21 min under visible light irradiation, which is much higher than that of Ag_3PO_4 (82%) on a per mole basis of Ag_3PO_4. The significant enhancement in the photocatalytic performance of EB–Ag_3PO_4 composites is ascribed not only to its high surface area, smaller size of the nanoparticles, adsorptivity and enhanced absorptivity in visible light but also to the electrostatic interaction between EB–Ag_3PO_4 and negatively charged exfoliated bentonite, the latter promoted the efficient migration of the photogenerated electrons and holes of Ag_3PO_4 and consequently improved the photocatalytic activity.

Acknowledgments

This work was supported by the National Natural Science Foundation of China (Grant No. 21477009), the Project of Jiangsu Province Industry-University-Research joint innovation fund (BY2013024-16) and Changzhou Science and Technology Development Program (CJ20140026). The TEM characterization was under the support of Dr. Xiazhang Li.

References

[1] Y. Bi, S. Ouyang, N. Umezawa, J. Cao, J. Ye, J. Am. Chem. Soc. 133 (2011) 6490–6492.
[2] X. Ma, B. Lu, D. Li, R. Shi, C. Pan, Y. Zhu, J. Phys. Chem. C 115 (2011) 4680–4687.
[3] Z.G. Yi, J.H. Ye, N. Kikugawa, T. Kako, S.X. Ouyang, H. Stuart-Williams, H. Yang, J.Y. Cao, W.J. Luo, Z.S. Li, Y. Liu, R.L. Withers, Nat. Mater. 9 (2010) 559–564.
[4] Y. Bi, H. Hu, Z. Jiao, H. Yu, G. Lu, J. Ye, Phys. Chem. Chem. Phys. 14 (2012) 14486–14488.
[5] P. Dong, Y. Wang, H. Li, H. Li, X. Ma, L. Han, J. Mater. Chem. A 1 (2013) 4651–4656.
[6] H. Wang, L. He, L.H. Wang, P.F. Hu, L. Guo, X.D. Han, J.H. Li, Crystengcomm 14 (2012) 8342–8344.
[7] H. Lin, H. Ye, B. Xu, J. Cao, S. Chen, Catal. Commun. 37 (2013) 55–59.
[8] G. Li, L. Mao, RSC Adv. 2 (2012) 5108–5111.
[9] Y. Wang, X. Li, Y. Wang, C. Fan, J. Solid State Chem. 202 (2013) 51–56.
[10] W. Liu, M.L. Wang, C.X. Xu, S.F. Chen, X.L. Fu, Mater. Res. Bull. 48 (2013) 106–113.
[11] L. Zhang, H. Zhang, H. Huang, Y. Liu, Z. Kang, New J. Chem. 36 (2012) 1541–1544.
[12] W. Yao, B. Zhang, C. Huang, C. Ma, X. Song, Q. Xu, J. Mater. Chem. 22 (2012) 4050–4055.
[13] X. Yang, H. Cui, Y. Li, J. Qin, R. Zhang, H. Tang, ACS Catal. 3 (2013) 363–369.
[14] Y. Ao, P. Wang, C. Wang, J. Hou, J. Qian, Appl. Surf. Sci. 271 (2013) 265–270.
[15] H.C. Zhang, H. Huang, H. Ming, H.T. Li, L.L. Zhang, Y. Liu, Z.H. Kang, J. Mater. Chem. 22 (2012) 10501–10506.
[16] P.F. Luckham, S. Rossi, Adv. Colloid Interface Sci. 82 (1999) 43–92.
[17] R. Zhu, Q. Chen, R. Zhu, Y. Xu, F. Ge, J. Zhu, H. He, Appl. Clay Sci. 107 (2015) 90–97.
[18] K.R. Ramakrishna, T. Viraraghavan, Water Sci. Technol. 36 (1997) 189–196.
[19] E. Eren, B. Afsin, J. Hazard. Mater. 151 (2008) 682–691.
[20] A.S. Ozcan, B. Erdem, A. Ozcan, Colloids Surf. A 266 (2005) 73–81.
[21] Y.J. Zhang, L.C. Liu, D.P. Chen, Powder Technol. 241 (2013) 7–11.
[22] M. Ghiaci, M.E. Sedaghat, H. Aghaei, A. Gil, J. Chem. Technol. Biotechnol. 84 (2009) 1908–1915.
[23] Y.P. Li, J. Zhan, L.Y. Huang, H. Xu, H.M. Li, R.X. Zhang, S.L. Wu, RSC Adv. 4 (2014) 11831–11839.
[24] J.G. Qu, N.N. Li, B.J. Liu, J.X. He, Mater. Sci. Semicond. Process. 16 (2013) 99–105.
[25] K.H. Hu, D.F. Zhao, J.S. Liu, Trans. Nonferrous Met. Soc. China 22 (2012) 2484–2490.
[26] J.F. Ma, J. Zou, L.Y. Li, C. Yao, T.L. Zhang, D.L. Li, Appl. Catal. B 134 (2013) 1–6.
[27] R. Zhu, W. Chen, T.V. Shapley, M. Molinari, F. Ge, S.C. Parker, Environ. Sci. Technol. 45 (2011) 6504–6510.
[28] X.L. Tan, J. Hu, X. Zhou, S.M. Yu, X.K. Wang, Radiochim. Acta 96 (2008) 487–495.
[29] S. Yang, D. Zhao, H. Zhang, S. Lu, L. Chen, X. Yu, J. Hazard. Mater. 183 (2010) 632–640.
[30] J. Li, W. Suyoulema, Sarina Wang, Solid State Sci. 11 (2009) 2037–2043.
[31] J. Tang, Z. Zou, J. Ye, Angew. Chem. Int. Ed. 43 (2004) 4463–4466.
[32] L. Liu, J. Liu, D.D. Sun, Catal. Sci. Technol. 2 (2012) 2525.
[33] J.F. Ma, L.Y. Li, J. Zou, Y. Kong, S. Komarneni, Micropor. Mesopor. Mater. 193 (2014) 154–159.
[34] A. Khan, M. Qamar, M. Muneer, Chem. Phys. Lett. 519–520 (2012) 54–58.
[35] J. Ma, J. Zou, L. Li, C. Yao, Y. Kong, B. Cui, R. Zhu, D. Li, Appl. Catal. B 144 (2014) 36–40.
[36] Y. Fujishiro, S. Uchida, T. Sato, Int. J. Inorg. Mater. 1 (1999) 67–72.
[37] X. Fu, Y. Hu, Y. Yang, W. Liu, S. Chen, J. Hazard. Mater. 244–245 (2013) 102–110.
[38] H. Katsumata, M. Taniguchi, S. Kaneco, T. Suzuki, Catal. Commun. 34 (2013) 30–34.
[39] S. Zhang, S. Zhang, L. Song, Appl. Catal. B 152–153 (2014) 129–139.
[40] J.J. Liu, X.L. Fu, S.F. Chen, Y.F. Zhu, Appl. Phys. Lett. 99 (2011) 191903.